Computational study of structural and elastic properties of random $Al_xGa_yIn_{1-x-y}N$ alloys

2010 J. Phys.: Condens. Matter 22 205801

(http://iopscience.iop.org/0953-8984/22/20/205801)

J. Phys.: Condens. Matter **22** (2010) 205801 (12pp) doi:10.1088/0953-8984/22/20/205801

Computational study of structural and elastic properties of random $Al_xGa_yIn_{1-x-y}N$ alloys

M Łopuszyński[1] and J A Majewski[2]

[1] Interdisciplinary Centre for Mathematical and Computational Modelling, University of Warsaw, Pawińskiego 5A, 02-106 Warsaw, Poland
[2] Institute of Theoretical Physics, Faculty of Physics, University of Warsaw, Hoża 69, 00-681 Warsaw, Poland

E-mail: m.lopuszynski@icm.edu.pl

Received 2 February 2010, in final form 30 March 2010
Published 26 April 2010
Online at stacks.iop.org/JPhysCM/22/205801

Abstract

In this work we present a detailed computational study of the structural and elastic properties of cubic $Al_xGa_yIn_{1-x-y}N$ alloys in the framework of the Keating valence force field model, for which we perform an accurate parametrization based on state-of-the-art density functional theory calculations. When analysing structural properties, we focus on the concentration dependence of the lattice constant, as well as on the distribution of the nearest and the next nearest neighbour distances. Where possible, we compare our results with experiment and calculations performed within other computational schemes. We also present a detailed study of the elastic constants for $Al_xGa_yIn_{1-x-y}N$ alloy over the whole concentration range. Moreover, we include the accurate quadratic parametrization for the dependence of the alloy elastic constants on the composition. Finally, we examine the sensitivity of the obtained results to computational procedures commonly employed in the Keating model for studies of alloys.

(Some figures in this article are in colour only in the electronic version)

1. Introduction

Recently AlN, GaN and InN have triggered much interest in optoelectronics, mostly because of their electronic structure, which makes them very promising materials for application in blue/green and UV active devices. Emitters and detectors operating in these spectral ranges can be used in many important areas such as optical data storage, biosensors, multimedia etc. Nitride alloys allow the continuous tuning of physical quantities such as band gap, lattice parameters, mobility etc, to reach suitable values for the desired applications.

Despite both theoretical and experimental efforts, many basic properties of nitride alloys are not yet sufficiently well understood. In this work, we focus on calculations of the structural and elastic properties of crystalline quaternary $Al_xGa_yIn_{1-x-y}N$ alloys, since they offer the greatest possibility of tuning. In particular, we examine the morphology of alloys, concentrating on the atomic distance distribution between the nearest and the next nearest neighbours. These are related to the electronic structure of alloys (see e.g. [1, 2]), which is crucial for application purposes. This knowledge is crucial for application purposes. In the case of the simpler ternary alloys AlGaN [3, 4], AlInN [5], GaInN [5–9], the bond length distributions have been obtained by extended x-ray absorption fine structure spectroscopy (EXAFS), however, for quaternary $Al_xGa_yIn_{1-x-y}N$ there are no available experimental data. As far as the elastic properties of alloys are concerned, their correct description is also a very important issue in modelling lasing from quantum wells, e.g. within $\boldsymbol{k}\cdot\boldsymbol{p}$ or similar continuous models. The nonlinear effects in elasticity of nitrides and their influence on properties of devices have recently attracted considerable attention [10–13]. However, there is not much known about the detailed dependence of the elastic properties on composition. In this paper, we present a computational study of the second-order elastic constants, c_{ij}, for crystalline $Al_xGa_yIn_{1-x-y}N$ quaternary alloys within the whole concentration range. This could provide a very useful insight from viewpoint of device modelling.

In the present study of quaternary nitride alloys, our main computational tool is the valence force field approach (VFF) developed by Keating [14]. Even though it was developed over forty years ago, it is still an important ingredient of multiscale models, particularly where a large number of alloy configurations needs to be handled. For nitrides, the Keating VFF model has recently been used to examine a plethora of physical phenomena, such as phonon spectra in bulk and in superlattices [15–17], structural properties of ternary bulk alloys [18–22] and their nanowires [23], the stability of different alloy phases [22] and also in numerous studies of thermodynamics of ternary [24–29] and quaternary [30] nitride alloys. Generally, the Keating VFF model is also a method of choice, where the atomic positions are needed as external input for electronic structure modelling. This is the case for methods atomistic in nature, but not entirely based on first principles, such as semiempirical tight-binding or empirical pseudopotential methods, that are commonly used for studies of low dimensional semiconductor structures. Therefore, to contribute to the further development and validation of the model, we also pay attention to the practical aspects of VFF usage. We compare the distribution of the nearest neighbour and next nearest neighbour distances resulting from the Keating VFF model with those obtained from accurate quantum-mechanical formalism, which is a good test of the VFF model reliability. We also examine the influence of the so-called mixing rule used to obtain VFF parameters for alloys, which shows how strongly this could influence prediction of the VFF model.

The paper is organized as follows. In section 2 we briefly recall basic facts about the Keating model and present the employed set of parameters. Section 3 provides a detailed overview of the structural properties for quaternary nitride alloys, it includes lattice constants as well as the distribution of the nearest neighbour and the next nearest neighbour distances. In this part we also compare the results of the Keating VFF with density functional theory (DFT) findings. In section 4, the VFF results for the elastic constants of $Al_xGa_yIn_{1-x-y}N$ alloys in the whole concentration range are presented. Section 5 deals with the computational procedures, the so-called mixing rule used to obtain the VFF parameters of alloys and the effect of finite supercell size. Finally, the paper is summarized in section 6.

2. Keating valence force field model and its parametrization

Keating [14], on the basis of general symmetry considerations, derived a potential energy model for zinc-blende type crystals in the following form

$$V(\boldsymbol{r}_1, \boldsymbol{r}_2, \ldots) = \sum_i \sum_{j \in NN(i)} \frac{3\alpha_{ij}}{16 d_{ij}^2} \left(\boldsymbol{r}_{ij}^2 - d_{ij}^2\right)^2 + \sum_i \sum_{\substack{j,k \in NN(i) \\ j \neq k}} \frac{3\beta_{ijk}}{16 d_{ij} d_{ik}} \left(\boldsymbol{r}_{ij} \cdot \boldsymbol{r}_{ik} + \frac{d_{ij} d_{ik}}{3}\right)^2. \quad (1)$$

Here, $\boldsymbol{r}_{ij} = \boldsymbol{r}_i - \boldsymbol{r}_j$, where $\boldsymbol{r}_i$, $\boldsymbol{r}_j$ denote the position of the ith and jth atoms respectively, d_{ij} denotes the equilibrium distance between atom i and j, $NN(i)$ represents the set of four nearest neighbours of the ith atom, α_{ij} and β_{ijk} stand for the force constants.

In the studies applying VFF to nitrides, very often a set of parameters proposed by Kim *et al* [31] is used. However, during recent years theoretical suggestions have appeared proposing a refined procedure for determination of the force constants in the VFF model [21]. On the other hand, an overall improvement of accuracy of the first principles computational methods has also been achieved. Therefore, we have decided to recalculate the force constants and bring them to the state-of-the-art.

The parametrization of the Keating VFF model starts from determination of the force constants α and β for bulk zinc-blende compounds. This can be done knowing the elastic constants of the bulks. As shown by Keating [14], the α and β are given by an analytic formula as a function of the elastic constants c_{11} and c_{12}. In the Keating model, the third elastic constant, i.e., c_{44}, is related to c_{11} and c_{12} as follows

$$\frac{2c_{44}(c_{11} + c_{12})}{(c_{11} - c_{12})(c_{11} + 3c_{12})} = 1. \quad (2)$$

Therefore, in the standard procedure to determine the α and β, c_{44} is not taken into account. However, equation (2) for the elastic constants resulting from the Keating model is not very well satisfied for nitrides. To improve this approach, Grosse and Neugebauer [21] proposed an alternative method. They suggested determining α and β by a least-squares fit to all three elastic constants. It turns out that such a fitting approach ensures a more uniform spreading of error and generally leads to better results. Therefore, we follow this approach in our work. Since the values of the elastic constants for zinc-blende nitrides have not been measured so far, we rely on theoretical predictions from the DFT based calculations. In our study, we take the arithmetic average of elastic constants obtained in the calculations within the DFT LDA and DFT GGA approximations to determine the force constants α and β. The elastic constants obtained through the averaging over these two theoretical schemes should be closer in value to experimental ones. This follows from the DFT LDA and DFT GGA tendencies to, respectively, overestimate and underestimate the stiffness of a material. The values of c_{ij} calculated within DFT GGA formalism have been taken from our previous work [12]. The DFT LDA estimates of c_{ij} have been calculated using the VASP package [32–34] and the projector augmented wave method [35]. The energy cutoff was set to 800 eV and the $11 \times 11 \times 11$ Monkhorst–Pack mesh [36] has been employed for the Brillouin zone integrals. The values of the elastic constants used for the fitting procedure are summarized in table 1, and the final set of employed parameters is shown in table 2.

Now we are in a position to determine parameters α_{ij} and β_{ijk} for the calculation of $Al_xGa_yIn_{1-x-y}N$ quaternary alloys. The values of the force constants α_{ij} are directly taken as the force constants α of a binary compound consisting of atomic species i and j. In the case of β_{ijk} three types of atoms can be involved, and obviously the parametrization, carried out for binary materials cannot determine these constants. In such cases we employ an arithmetic mixing rule, i.e., take the

Table 1. Elastic constants used to parametrize the Keating model.

	c_{11}	c_{12}	c_{44}	
AlN	301	167	188	LDA
	282	149	179	GGA, see [12]
GaN	288	159	161	LDA
	252	129	147	GGA, see [12]
InN	184	127	84	LDA
	159	102	78	GGA, see [12]

Table 2. Set of parameters for the Keating VFF model employed in the present study.

	d (Å)	α (N m^{-1})	β (N m^{-1})
AlN	1.894	79.91	19.73
GaN	1.950	76.25	17.80
InN	2.165	62.07	9.68

arithmetic average of suitable binary parameters, as has been applied in many previous works, e.g. [19, 25, 26]. Specifically, this means that $\beta_{\mathrm{Ga,N,In}} = (\beta_{\mathrm{Ga,N,Ga}} + \beta_{\mathrm{In,N,In}})/2$, and so on. However, there is also the possibility to use a geometric average instead (see e.g. Schabel and Martins [37] or Saito and co-workers [20]). We investigate the role of employed mixing rule later on (see section 5 for details).

3. Structural properties from the VFF model and their comparison with DFT calculations

In this section, we analyse the composition dependence of the structural properties and geometry of crystalline $Al_xGa_yIn_{1-x-y}N$ alloys (i.e., lattice constants, the nearest and next nearest neighbour distances). The distribution of bond lengths in the alloy can be also extracted from EXAFS experiments, which is a useful crosscheck for the theory. The local geometry of the alloy is an important issue, since it correlates with the electronic structure, see e.g. recent calculations of Gorczyca *et al* [1, 2] for nitride alloys. The Keating VFF model is particularly suitable for the task of establishing the local environment of random alloys. It enables calculations with large supercells, which in turn guarantee reasonably good sampling and randomness of alloys. There is fairly long history of employing VFF models to determine the alloy geometry for various types of materials. For example, Cai and Thorpe studied relaxation patterns in quaternary $A_{1-x}B_xC_{1-y}D_y$ [38] and general ternary $A_{1-x}B_xC$ alloys [39] using the Kirkwood model very similar to the Keating VFF approach. Schabel and Martins [37] gave a detailed overview of the structure for a very broad range of semiconducting alloys within the Keating VFF. Their work, however, does not include nitrides. The structure of ternary nitride alloys has been also studied by many other authors [18–20]. In this work, we present the first VFF study of structure for quaternary nitride alloys. We compare our results for bond length distribution with the recent calculations of Marques *et al* [40] carried out within the generalized quasichemical approximation (GQCA). Where possible we also compare our findings with experimental data, obtained using the EXAFS approach. To shed some light on the accuracy of the Keating VFF, we also compare the structural properties of this force field model with accurate DFT calculations. The latter treatment allows only for calculations with moderate sizes of supercells. On the other hand the DFT description of interactions between atoms is very complete. Therefore, such a comparison can reveal the potential weak points of a fully local classical description. Since the VFF model is widely used to provide geometry to semiempirical calculations of electronic structure handling large systems (e.g. tight-binding or empirical pseudopotential schemes), the question of its accuracy is important. Obviously, the quality of such a multiscale approach depends on the accuracy of the input structures, however, to the best of our knowledge, no detailed comparison of VFF with more accurate models (e.g. DFT) has been so far presented in the literature.

3.1. Computational details

For VFF simulations, we used $18 \times 18 \times 18$ zinc-blende cubic supercells containing 46 656 atoms with a random distribution of cations. We optimized both the atomic positions and the lattice constant of the cubic cell. For the DFT simulations, we employed the VASP package [32–34]. We used the local density approximation for the exchange and correlation functional according to Ceperley and Alder [41]. The projector augmented wave method was used in its variant available in the VASP code [35]. The calculations were performed for $3 \times 3 \times 3$ zinc-blende cubic cells containing 216 atoms. Also in this case the cation distribution among sites was random. The energy cutoff was set to 550 eV. For Brillouin zone sampling, only the Γ point was used due to the large supercell size.

3.2. Lattice constant

In the early 20th century Vegard noticed that lattice constants for alloys can be calculated using linear interpolation between the lattice constants of their constituents [42]. Nitride alloys follow this so-called Vegard's law, which has been confirmed by a series of experimental findings, see e.g. a recent experiment for GaInN nanowires, where the linear dependence of the lattice constant was observed in the whole concentration range [43].

The results of our simulations for lattice constant are presented in figure 1. One can easily observe that DFT LDA formalism reproduces very well the linear Vegard-like behaviour, even though the LDA approximation is well known to systematically underestimate the values of lattice constants. On the other hand the Keating VFF predicts some bowing in the dependence of lattice constant on concentration. This is in accordance with the work of Thorpe and co-workers [44], who analysed Vegard's law for a simple VFF-like model. In their case they showed that Vegard's law is obtained when force constant disorder is neglected. Therefore, since in our calculations force constant disorder is included (i.e., α and β depend on the types of atoms considered), it is possible to expect deviations from linearity. This is a feature of the Keating VFF method; however, as can be seen from figure 1, its magnitude is not very large.

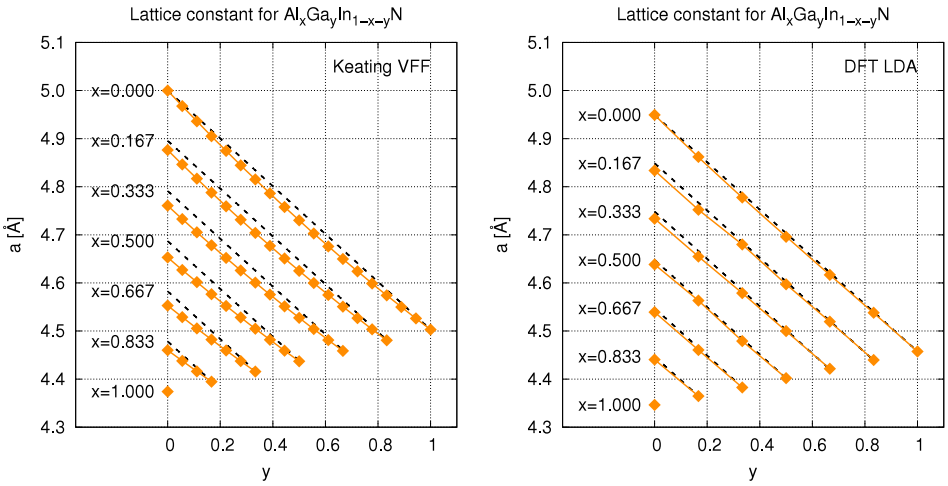

Figure 1. Comparison of lattice constants dependence on the alloy composition for $Al_xGa_yIn_{1-x-y}N$ obtained using the Keating VFF (left panel) and DFT LDA (right panel). Points correspond to results of calculations, solid lines are only to guide the eye. Dashed lines denote the prediction of Vegard's law. Note that for convenient comparison the scale on both graphs is the same.

Table 3. Results of the linear fits to average nearest neighbour distances for $Al_xGa_yIn_{1-x-y}N$ quaternary alloys.

Bond	Model	Fit function	Error (%)	Ref.
Al–N	VFF	$1.9496 - 0.054\,96\,x - 0.038\,93\,y$	0.10	This work
	DFT LDA	$1.9279 - 0.044\,19\,x - 0.043\,14\,y$	0.26	This work
	GQCA	$1.9435 - 0.050\,90\,x - 0.054\,55\,y$	0.19	[40]
Ga–N	VFF	$1.9959 - 0.063\,22\,x - 0.045\,73\,y$	0.10	This work
	DFT LDA	$1.9762 - 0.043\,67\,x - 0.044\,70\,y$	0.27	This work
	GQCA	$1.9919 - 0.059\,85\,x - 0.060\,50\,y$	0.35	[40]
In–N	VFF	$2.1676 - 0.098\,99\,x - 0.074\,85\,y$	0.12	This work
	DFT LDA	$2.1461 - 0.052\,76\,x - 0.050\,88\,y$	0.21	This work
	GQCA	$2.1573 - 0.082\,92\,x - 0.075\,70\,y$	0.55	[40]

3.3. Nearest neighbour distance

Results of calculations of the nearest neighbour distance dependence on concentration of alloy constituents for $Al_xGa_yIn_{1-x-y}N$ are presented in figure 2. It is well known that even though the lattice constants obey Vegard's law, the individual bond lengths do not follow this simple rule. The dependence of bond lengths on concentration is usually also linear, however, bond lengths remain much closer to their original bond length in bulk binary material, rather than to the average bond length predicted by a Vegard-like law (see e.g. [45, 46]). This linear dependence of the bond lengths in the alloy on the concentration of Al and Ga cations, x and y respectively, can be described by the linear form

$$d(x, y) = d_0 + Ax + By. \tag{3}$$

The coefficients A and B in equation (3) have been determined by fitting the bond lengths obtained from both the Keating and LDA schemes. These linear fits are represented by the dashed lines in figure 2. The small values of coefficients A and B (see table 3 gathering results of fitting procedure for all types of bonds) allow even for very rough approximation of $d(x, y)$ by d_0, just confirming the statement about bond lengths made above.

On the basis of the presented plots (figure 2) for bond lengths in $Al_xGa_yIn_{1-x-y}N$ alloy, one can compare findings of the Keating VFF model with the DFT LDA approach. Results of both computational methods can be reasonably well described by a linear dependence of the bond lengths on the cation concentrations given by equation (3). Naturally, since the DFT LDA calculations have been performed for much smaller cell sizes (histograms were generated on the basis of two 216 atoms supercell calculations) the data have a larger statistical error than the Keating VFF computations. This effect is particularly pronounced in those parts of the graphs where a low concentration of considered cation is present in the sample. The second evident observation is that DFT LDA bond lengths are systematically shifted towards lower values than the Keating VFF. This is related to the well known LDA flaw to underestimate the lattice constants. It is also worth noticing that the results of previous computations by Marques *et al* [40], which have been carried out within the generalized quasichemical approximation (GQCA), are in particularly good agreement with the findings of the Keating VFF model (see table 3 for details).

Another interesting aspect is to compare the probability distribution profiles predicted by both the DFT LDA and Keating VFF models. Two sample histograms generated by both models are depicted in figure 3. One can see that both schemes lead to results that are in satisfactory agreement with each other. It is again clear that DFT LDA systematically

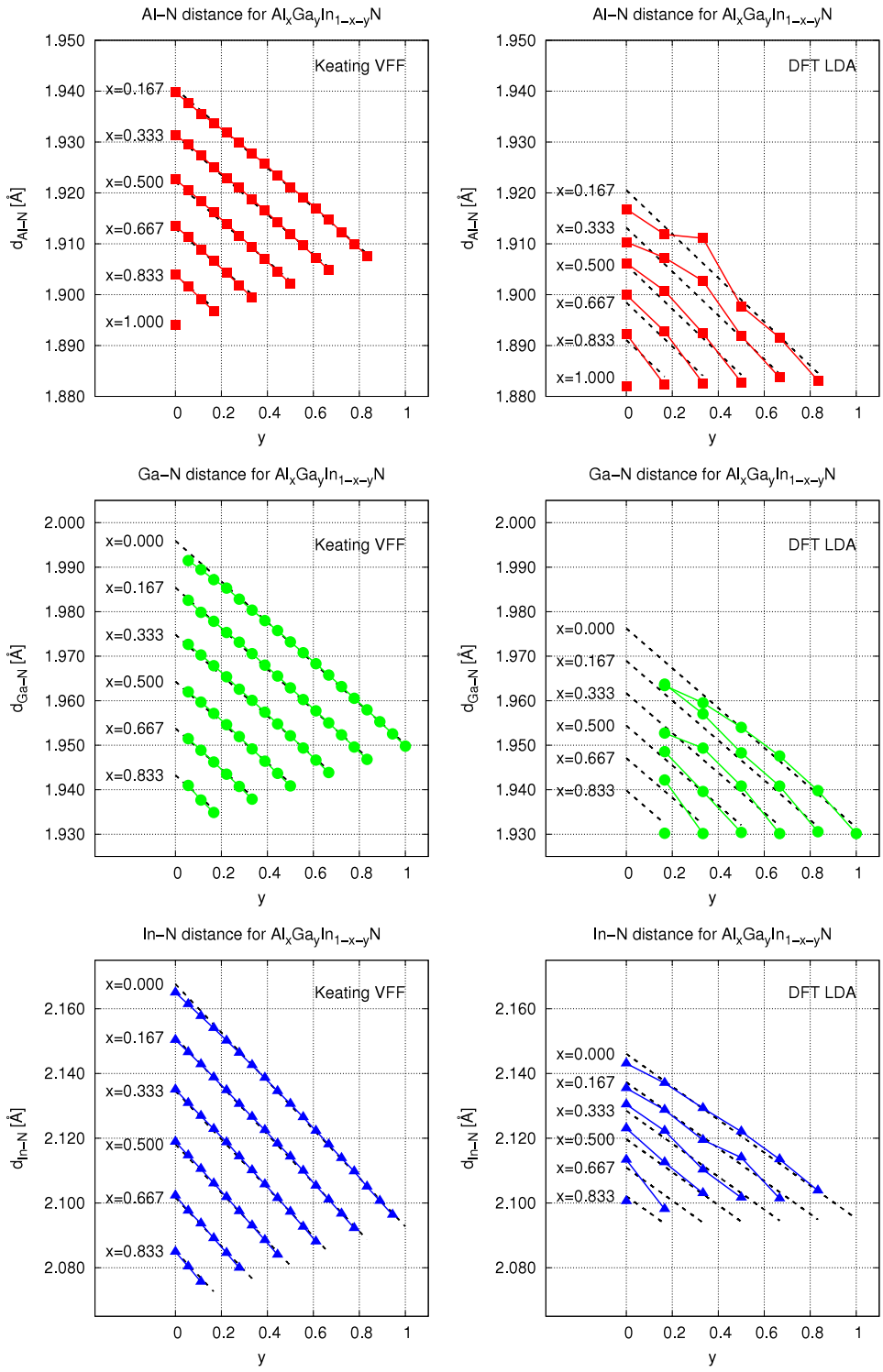

Figure 2. The dependence of the average bond length on alloy composition for $Al_xGa_yIn_{1-x-y}N$ obtained using the Keating VFF and DFT LDA schemes. Points correspond to the results of calculations, solid lines are only to guide the eye. Dashed lines denote linear fits presented in table 3. Note that for convenient comparison the scale on the Keating VFF and DFT LDA graphs is the same.

underestimates the bond lengths, so the peaks corresponding to each bond type are shifted towards lower values. One can also notice that the Keating VFF model predicts larger peak widths than the DFT LDA approach does. Particularly interesting are cases of high In concentration. There, one can observe rather large lattice deformations caused mostly by the considerable lattice mismatch between InN and GaN or AlN. This can be considered as a test of the Keating VFF, which has been parametrized on the basis of elastic constants c_{ij}, i.e., taking into account the second-order effects in deformation strain, which, in principle, describe the material behaviour in the regime of small deformations. However, also for these

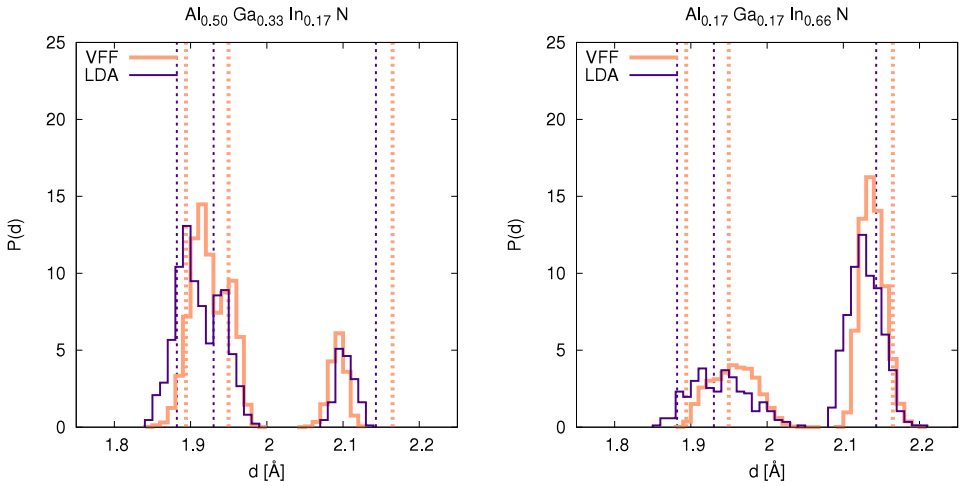

Figure 3. The nearest neighbour distance distribution resulting from the Keating VFF and DFT LDA for $Al_{0.50}Ga_{0.33}In_{0.17}N$ and $Al_{0.17}Ga_{0.17}In_{0.66}N$ random alloys. Vertical dashed lines denote the nearest neighbour distance in pure AlN, GaN and InN respectively as predicted by both presented models.

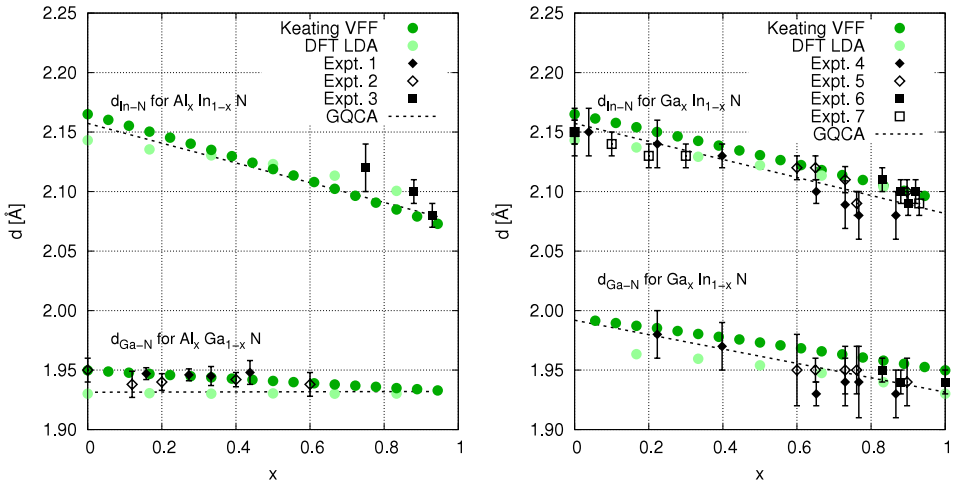

Figure 4. Comparison of our theoretical results obtained within both DFT LDA and Keating VFF models with various experimental data. The measurements from the following works are included: for $Al_xGa_{1-x}N$ Expt. 1—Miyano *et al* [3], Expt. 2—Yu *et al* [4], for $Al_xIn_{1-x}N$ Expt. 3—Katsikini *et al* [5], for $Ga_xIn_{1-x}N$ Expt. 4—MBE samples of Kachkanov *et al* [8], Expt. 5—MOCVD samples of Kachkanov *et al* [8], Expt. 6—Katsikini *et al* [7], Expt. 7—Katsikini *et al* [5]. The results of previous theoretical predictions within GQCA [40] are presented for completeness.

cases, the agreement is reasonable, in spite of neglecting higher order contributions to the elastic energy (see e.g. results for $Al_{0.17}Ga_{0.17}In_{0.66}N$ presented in figure 3).

Finally, it is interesting to examine how the presented theoretical results agree with experiments. We are not aware of any experimental results for bond length distribution in $Al_xGa_yIn_{1-x-y}N$ alloys, however, there is a significant body of experimental data for ternaries $Al_xGa_{1-x}N$, $Al_xIn_{1-x}N$, and $Ga_xIn_{1-x}N$. A comparison of the experimental bond lengths in ternary alloys with predictions of the Keating VFF model is presented in figure 4. Even though measurements are performed for wurtzite samples, the comparison with the theoretical predictions for cubic phases is reasonable, owing to the local similarity of both crystallographic phases. In wurtzite structures, the nearest neighbour bond elongations in the direction of the crystallographic *c*-axis are typically of the order of 0.01 Å [2, 47]. This is very similar to typical experimental error bars or bond length spread resulting from disorder in alloys (compare histogram in figure 3). As can be seen in figure 4, the comparison of available data with our theoretical results reveals good agreement. It could be, of course, interesting to see how this relates to the structural properties of cubic $Al_xGa_yIn_{1-x-y}N$ whose growth using molecular beam epitaxy was recently reported [48]. For completeness, in figure 4 we have also included the DFT findings, which again show the well known systematic tendency to underestimate the bond lengths.

3.4. Next nearest neighbour distance

Here we analyse the closest distances between atoms of the same (cationic or anionic) sublattice, i.e., the next nearest

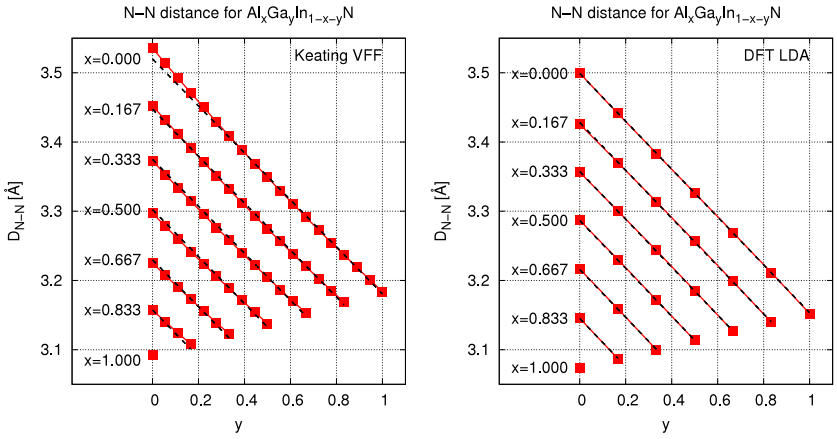

Figure 5. The average next nearest neighbour distances as a function of composition for $Al_xGa_yIn_{1-x-y}N$ obtained using the Keating VFF and DFT LDA, for the case of nitrogen–nitrogen. Points correspond to results of calculations, solid lines are only to guide the eye. Dashed lines denote the linear fits presented in the table 4. Note that for convenient comparison the scale on both graphs is the same.

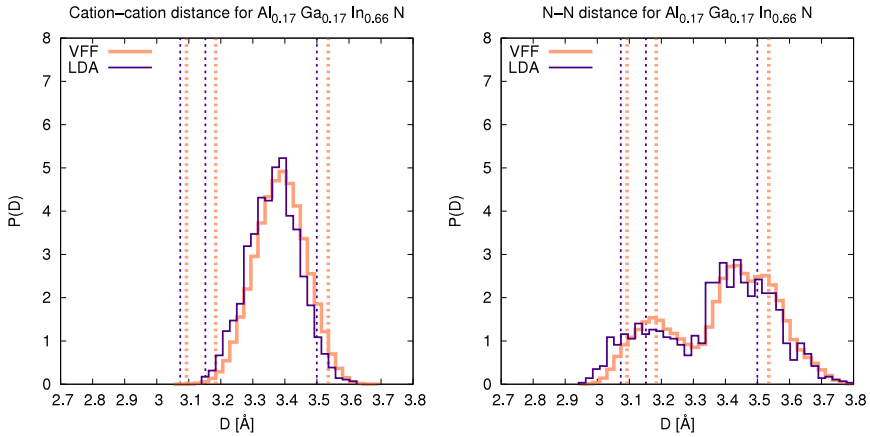

Figure 6. Comparison of the next nearest neighbour distance distribution resulting from the Keating VFF and DFT LDA for $Al_{0.17}Ga_{0.17}In_{0.66}N$. Vertical dashed lines denote the next nearest neighbour distance in pure AlN, GaN and InN respectively as predicted by both presented models.

neighbour distance of an anion or cation. The results obtained within both VFF and DFT models for a nitrogen–nitrogen pairs are presented in figure 5. Qualitatively, the results for the smallest distances of the cationic pairs are very similar, exhibiting a dominantly linear dependence on the concentration of the constituents. The coefficients A and B that determine this linear dependence (see equation (3)) are presented in the table 4 for both cation–cation and nitrogen–nitrogen average distance. The maximum error of the fit is also included there. Since in modern EXAFS experiments it is possible to measure the cation–cation distances for every distinct pair separately, we have also performed the fits for all possible combinations of cation–cation distances, namely Al–Al, Al–Ga, Al–In, Ga–Ga, Ga–In, In–In (see table 5). Again, in all cases a linear model provides satisfactory description.

In addition to the dependence of average cation–cation and anion–anion distance on concentration, we have also analysed the shape of the distribution. Sample histograms are depicted in figure 6. When inspecting the presented graphs, one can notice that the cationic and nitrogen sublattices relax in a different manner. The behaviour of the cation–cation distribution is similar to a virtual crystal exhibiting a unimodal shape. At the same time the nitrogen–nitrogen distance is much more distorted with respect to the single-peaked virtual crystal picture. The shape of the distribution is multimodal. The peaks correspond to three possible combinations of a N–N pair joined by a Al, Ga or In atom respectively. Since the equilibrium distances of Al–N and Ga–N are very similar, the pairs of N–N joined by Al and Ga form a common maximum on the presented plot. These findings agree very well with the same behaviour reported for ternaries [19, 37]. Comparing the bond

Table 4. Results of linear fit to the average next nearest neighbour cation–cation (CT–CT) and nitrogen–nitrogen (N–N) distances for $Al_xGa_yIn_{1-x-y}N$ quaternary alloys.

Distance	Model	Fit function	Max. error (%)
CT–CT	VFF	$3.5147 - 0.432\,34\,x - 0.335\,00\,y$	0.59
	DFT LDA	$3.4934 - 0.422\,43\,x - 0.341\,07\,y$	0.18
N–N	VFF	$3.5200 - 0.435\,17\,x - 0.339\,31\,y$	0.44
	DFT LDA	$3.4991 - 0.424\,87\,x - 0.345\,62\,y$	0.07

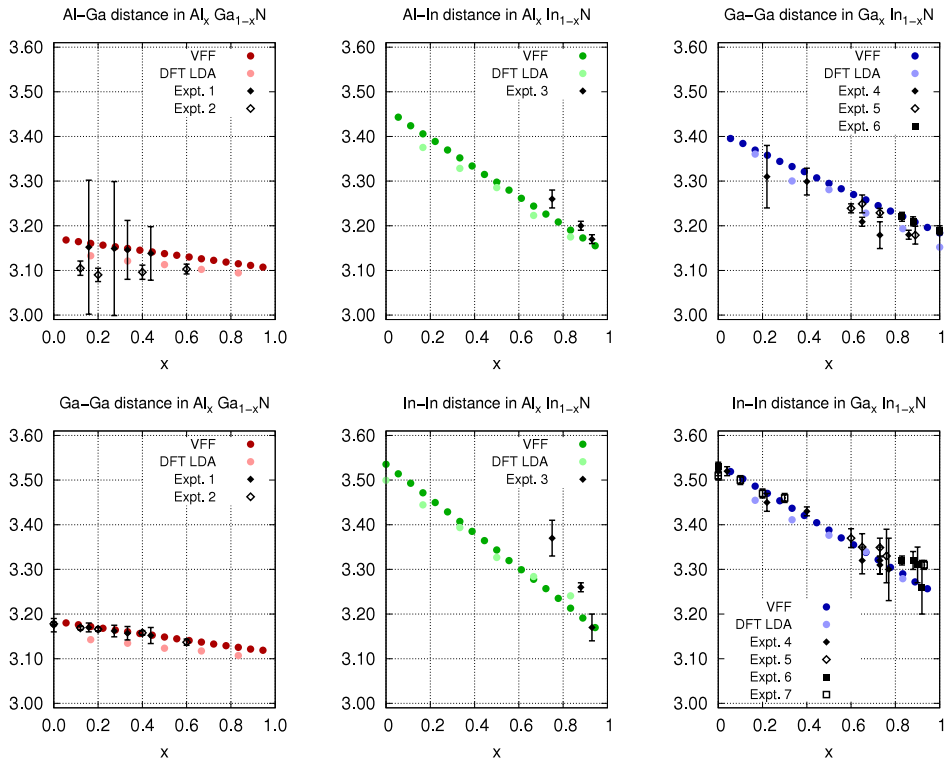

Figure 7. Comparison of our theoretical results for average next nearest neighbour distances with various experimental findings: for $Al_xGa_{1-x}N$ Expt. 1—Miyano *et al* [3], Expt. 2—Yu *et al* [4], for $Al_xIn_{1-x}N$ Expt. 3—Katsikini *et al* [5], for $Ga_xIn_{1-x}N$ Expt. 4—MBE samples of Kachkanov *et al* [8], Expt. 5—MOCVD samples of Kachkanov *et al* [8], Expt. 6—Katsikini *et al* [7], Expt. 7—Katsikini *et al* [5]. All distances are in Angstroms.

Table 5. Results of linear fits to the average next nearest neighbour distances between various pairs of cations for $Al_xGa_yIn_{1-x-y}N$ quaternary alloys.

Distance	Model	Fit function	Max. error (%)
Al–Al	VFF	$3.3660 - 0.274\,16\,x - 0.206\,66\,y$	0.15
	DFT LDA	$3.3663 - 0.290\,78\,x - 0.237\,71\,y$	0.78
Al–Ga	VFF	$3.3865 - 0.283\,85\,x - 0.214\,59\,y$	0.07
	DFT LDA	$3.3798 - 0.295\,93\,x - 0.236\,51\,y$	0.24
Al–In	VFF	$3.4599 - 0.323\,54\,x - 0.246\,85\,y$	0.05
	DFT LDA	$3.4286 - 0.306\,25\,x - 0.235\,13\,y$	0.31
Ga–Ga	VFF	$3.4057 - 0.293\,38\,x - 0.221\,79\,y$	0.18
	DFT LDA	$3.3922 - 0.291\,27\,x - 0.239\,31\,y$	0.43
Ga–In	VFF	$3.4771 - 0.334\,79\,x - 0.255\,54\,y$	0.06
	DFT LDA	$3.4474 - 0.304\,69\,x - 0.249\,91\,y$	0.26
In–In	VFF	$3.5362 - 0.387\,25\,x - 0.297\,34\,y$	0.11
	DFT LDA	$3.4983 - 0.312\,51\,x - 0.260\,31\,y$	0.53

length histograms obtained within the VFF and DFT schemes (see figure 6), it is interesting to note that the agreement in the predicted next nearest neighbour distances is in this case even better than for the nearest neighbour histograms. To some extent it is caused by the fact that the larger peak widths than in the case of the nearest neighbour distance distributions cause the systematic differences between bond length predicted by DFT and VFF to be less pronounced. Since the VFF model includes explicit interactions only between the nearest neighbours, one could think that the description of a second coordination shell would be less accurate. However, it turns out that the VFF model also provides very reliable predictions for cation–cation and anion–anion distances (see figure 6).

Even though the experimental data for quaternaries are unavailable, similarly to in the nearest neighbour case, there are a considerable number of results for ternaries. The comparison of experimental findings with our theoretical results is presented in figure 7. Generally, the agreement is very good, however, a few things are worth pointing out here. One can notice that quite often the results measured by different groups exhibit significant spread and, in addition, some of the experimental data exhibit large error bars. This underlines the fact that such measurements are at the edge of available experimental techniques. The largest discrepancies between theory and experiment we observe for $Al_xIn_{1-x}N$ alloy (see the middle column of the graph 7), however, there is only one recent report [5] known to us which deals with the structure of this material. To elucidate the matter, more experimental data would be very helpful. One has also to bear in mind that our calculation assume a random cation distribution in the sample. If some kind of clustering for a particular type of cations occurs, it could lead to modification of the presented results.

4. Elastic constants for alloys calculated using the Keating model

In this section we present results of calculations of elastic constants c_{ij} for random $Al_xGa_yIn_{1-x-y}N$ alloys. Calculations

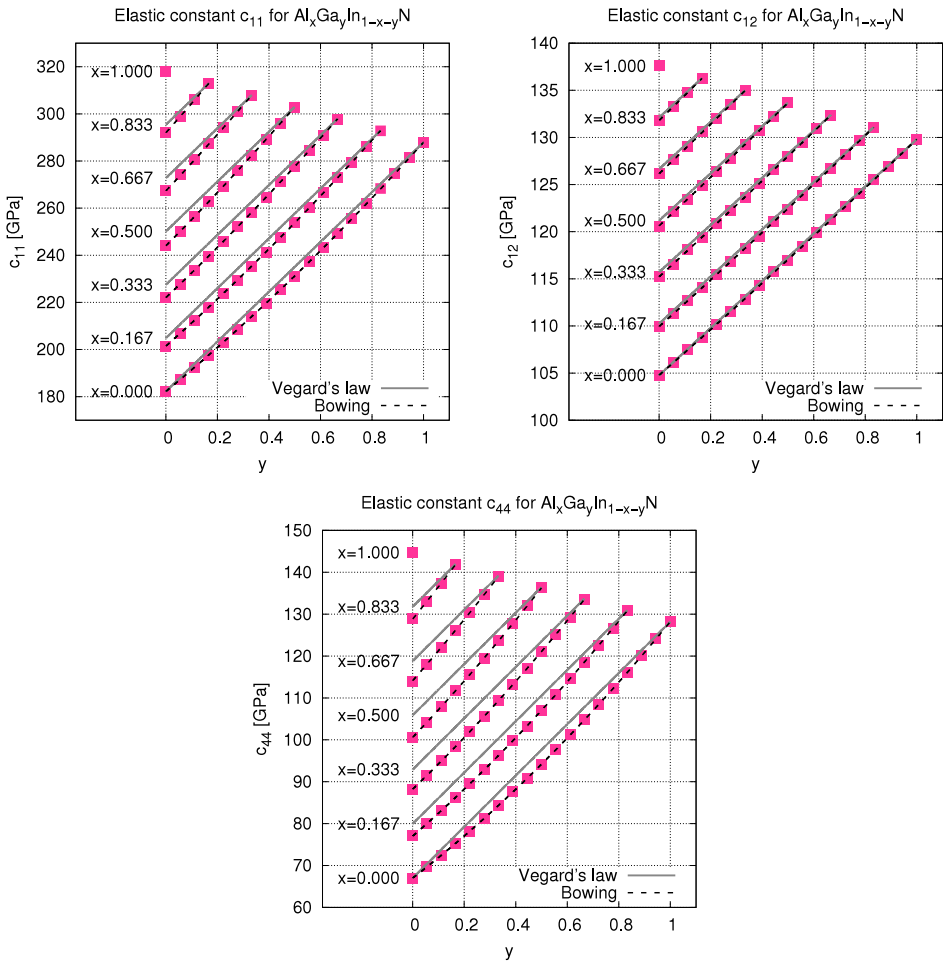

Figure 8. Elastic constants dependence on composition for $Al_xGa_yIn_{1-x-y}N$ alloys calculated on the basis of the Keating VFF.

were carried out using the Keating VFF and cover the whole concentration range. To extract the values of the alloy elastic constants, we have applied three types of strains to every alloy supercell:

$$\begin{aligned} \boldsymbol{\epsilon}_A &= [\epsilon, 0, 0, 0, 0, 0], \\ \boldsymbol{\epsilon}_B &= [\epsilon, -\epsilon, 0, 0, 0, 0], \\ \boldsymbol{\epsilon}_C &= [0, 0, 0, 0, 0, \epsilon]. \end{aligned} \tag{4}$$

For each type of the deformation ϵ has been varied within the range of values $\{-1.0\%, -0.5\%, 0.5\%, 1\%\}$ and the elastic energy has been calculated. Then, on the basis of strain-energy relation

$$E = \frac{1}{V_0} \sum_{i,j=1}^{6} c_{ij} \epsilon_i \epsilon_j, \tag{5}$$

three elastic constants c_{11}, c_{12} and c_{44} have been determined from parabolic fits to the energy for deformations $\boldsymbol{\epsilon}_A, \boldsymbol{\epsilon}_B, \boldsymbol{\epsilon}_C$.

The results are presented in figure 8. We also include there the prediction of a Vegard-like law for elastic constants:

$$c_{ij}^{\text{Vegard}}(x, y) = x\, c_{ij}^{\text{AlN}} + y\, c_{ij}^{\text{GaN}} + (1 - x - y)\, c_{ij}^{\text{InN}}. \tag{6}$$

The exact functional forms of this equation for c_{11}, c_{12} and c_{44} are explicitly given in table 6. However, after a brief analysis of graph 8, one notices that the Keating VFF results are not very well described by the above Vegard's law. This is particularly pronounced for elastic constants c_{11} and c_{44}. The deviation for c_{12} is very weak, but this elastic constant also has the lowest discrepancy between materials AlN, GaN and InN. To fully describe the dependence of c_{ij} on composition one has to include a bowing term $\Delta c_{ij}(x, y)$, which is defined as follows:

$$\begin{aligned} c_{ij} &= c_{ij}^{\text{Vegard}}(x, y) + \Delta\, c_{ij}(x, y), \\ \Delta\, c_{ij}(x, y) &= P\, x(1 - x) + Q\, xy + R\, y(1 - y). \end{aligned} \tag{7}$$

After including this additional function and performing a fitting procedure for P, Q and R, the VFF results are reproduced with an accuracy much better than 1 GPa. The coefficients P, Q, and R for the cubic elastic constants are provided in table 6.

The literature indicates that bowing in the alloy elastic constants c_{ij} should indeed be expected. Chen and Sher in their book [46] point out that the value of Δc_{ij} should be always negative, which is the case in our studies. They argue that since the elastic properties of semiconductors correlate with the inverse power of the lattice constant and that lattice constants for alloys follow Vegard's law, then the c_{ij} dependence on composition should be sublinear. They also perform a simple analysis within the framework of the Keating VFF model, showing that, for simple ordered structures, sublinear bowing

Table 6. Concentration dependence of the elastic constants c_{ij} for $Al_xGa_yIn_{1-x-y}N$ alloys. The accuracy of the linear Vegard-like model is compared with fits including an additional bowing term Δc_{ij}. All data in GPa.

	Result of fit for c_{ij}	Max. difference: (GPa)	
c_{11}	Vegard's law		
	$182.23 + 135.79\,x + 105.70\,y$	6.2	(2.6%)
	Vegard's law + bowing term Δc_{11}		
	$\Delta c_{11} = -24.51\,x(1-x) + 39.70\,xy - 15.44\,y(1-y)$	0.3	(0.1%)
c_{12}	Vegard's law		
	$104.78 + 32.80\,x + 25.02\,y$	0.7	(0.6%)
	Vegard's law + bowing term Δc_{12}		
	$\Delta c_{12} = -2.22\,x(1-x) + 3.10\,xy - 1.00\,y(1-y)$	0.1	(0.1%)
c_{44}	Vegard's law		
	$67.00 + 77.71\,x + 61.20\,y$	5.3	(5%)
	Vegard's law + bowing term Δc_{44}		
	$\Delta c_{44} = -21.06\,x(1-x) + 33.99\,xy - 13.68\,y(1-y)$	0.1	(0.1%)

in bulk modulus is present. Also, our preliminary calculations within the virtual crystal DFT pseudopotential scheme (VCA DFT, sometimes referenced as computational alchemy) predict the presence of the bowing term in $c_{ij}(x, y)$ [49]. However, one has to bear in mind that VCA DFT works best for alloys where the lattice mismatch of the constituents is low. A larger mismatch, as in the case of InN with both AlN and GaN, can introduce a considerable inaccuracy to this model.

To summarize this section, we have shown that the Keating VFF model predicts a quadratic dependence of the elastic constants c_{ij} on $Al_xGa_yIn_{1-x-y}N$ alloy composition. This effect is in agreement with the previous literature studies [46, 49]. We believe that, even though the effect is not very large, the awareness of it could improve description and modelling of devices based on low dimensional nitride structures, such as quantum dots and quantum wells. When the elastic constants of the more common wurtzite phase of $Al_xGa_yIn_{1-x-y}N$ are needed, one can obtain the dependencies for this phase using the Martin transformation [50] to the data gathered in table 6. It would be also interesting to compare the presented results with other modelling approaches, since the Keating VFF is a simple tool and does not capture many effects. Accurate experimental studies would also be of great value here. Finally, one has to stress the fact that the above results apply to crystalline samples, e.g. such as those grown within MBE method by As *et al* [48]. Polycrystalline and amorphous phases require different computational approaches.

5. Influence of the mixing rule and finite supercell size

In this section we give a brief overview of two more technical aspects of the presented calculations. First, we examine to what extent the results of our VFF alloy simulations are sensitive to the selection of the mixing rule. Second, we analyse how effects of finite supercell size influence the structural properties.

As already mentioned in section 2, following e.g. [19, 25, 26] and many other works, we have used an arithmetic mixing rule to interpolate between the three-body β constants of base materials, i.e.,

$$\beta_{\mathrm{Al,N,Ga}} = \frac{\beta_{\mathrm{Al,N,Al}} + \beta_{\mathrm{Ga,N,Ga}}}{2} \tag{8}$$

and so on. Obviously this is not the only option. Therefore, an important question arises—to what extent does this choice influence the results presented so far? In order to check this, we carried out a set of simulations for geometric mixing, used e.g. by Schabel and Martins [37] or Saito *et al* [20]. This means that instead of equation (8) we have:

$$\beta_{\mathrm{Al,N,Ga}} = \sqrt{\beta_{\mathrm{Al,N,Al}}\,\beta_{\mathrm{Ga,N,Ga}}} \tag{9}$$

and so on. Other Keating VFF parameters are left unchanged.

Sample results of this numerical experiment are presented in figure 9. Generally, it turns out that average lengths remain virtually unaffected by the type of mixing. In the left panel of figure 9, where the average In–N distance is presented, one can see that the curves for the arithmetic and geometric mixing almost cover each other. This is because the difference there does not exceed 0.05%. The behaviour is similar for both average nearest neighbour and next nearest neighbour distances. Small differences could be observed in the results for the elastic constants. The maximum deviations were: $\Delta c_{11} = 1.4$ GPa (0.6%), $\Delta c_{12} = 0.5$ GPa (0.4%), $\Delta c_{44} = 1.4$ GPa (1.3%). It turns out that c_{11} and c_{44} are always larger in the arithmetic than in the geometric mixing model, whereas for c_{12}, it is the other way round. A graphical comparison of the c_{44} dependence on concentration in both approaches is depicted in the right panel of figure 9. Even though the results for the elastic properties depend on the type of mixing used, the differences are really very small, strongly suggesting that both ways of mixing constants β lead to equally valuable predictions. A detailed verification of which rule works better would be rather difficult, requiring very accurate experimental investigations.

Another interesting technical aspect of the presented simulations is verification to what extent the finite cell size influences the obtained results. Particularly, one may wonder if results obtained on the basis of two $3 \times 3 \times 3$ supercells per concentration in DFT LDA calculations (section 3) reproduce

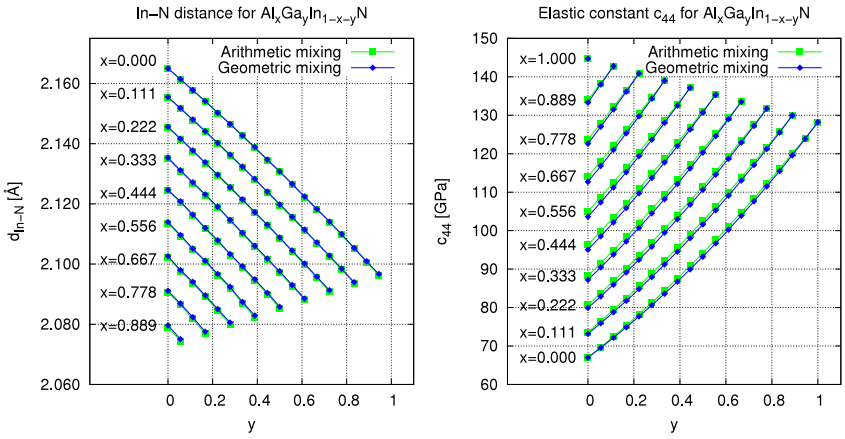

Figure 9. Comparison of calculation results using the VFF model with different mixing rules—arithmetic and geometric. Left panel presents $d_{\mathrm{In–N}}(x, y)$, the results for arithmetic and geometric mixing are so close to each other that it is impossible to distinguish them in the figure. The right panel presents a similar comparison for the elastic constant $c_{44}(x, y)$.

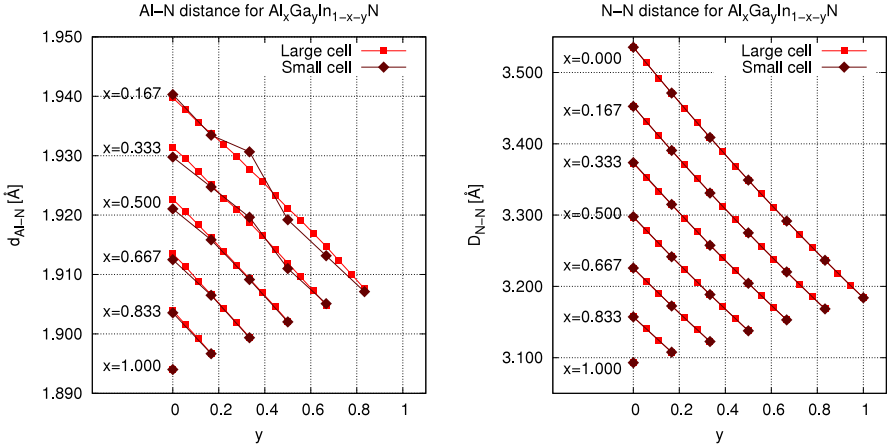

Figure 10. Comparison of calculation results using the VFF model with different cell sizes. Small cell size corresponds to data gathered from two different $3 \times 3 \times 3$ cubic cells (216 atoms each), large cell size corresponds to $18 \times 18 \times 18$ cubic cell (46 656 atoms). Right panel compares nearest neighbour distance $d_{\mathrm{Al–N}}(x, y)$ and left panel presents next nearest neighbour distance $D_{\mathrm{N–N}}(x, y)$. The latter results for both considered sizes are so close that they are impossible to distinguish in the picture.

sufficiently well the properties of random alloy. To verify this, we computed geometries of the same small cells used for DFT LDA calculations by means of the VFF model. The comparison of data obtained for these small cells with our VFF results for $18 \times 18 \times 18$ supercells (46 656 atoms) is presented in figure 10. One can see that on the sample diagram of nearest neighbour distance $d_{\mathrm{Al–N}}$, even though differences are present, they have the form of typical statistical noise preserving the same linear trends as has been found for large supercells. The same behaviour was observed for other pairs of nearest neighbours. The analysis of the next nearest neighbour distances reveals even better agreement. This is because the second coordination shell in zinc-blende (or ideal wurtzite) contains 12 atoms, whereas the first consists of only four nearest neighbours. This increases the statistics and leads to smaller error for the next neighbours. On the basis of the presented comparison, one can conclude that $3 \times 3 \times 3$ supercells reproduce correctly the trends observed in the structural properties for much larger systems.

6. Summary

In this work we have presented a computational study of the structural and elastic properties of zinc-blende quaternary $\mathrm{Al}_x\mathrm{Ga}_y\mathrm{In}_{1-x-y}\mathrm{N}$ alloys over the whole concentration range. Our main computational tool was the Keating VFF model. We started by presenting a new parametrization of this model based on state-of-the-art quantum-mechanical calculations within DFT formalism. Then we showed the VFF results for the lattice constant and distributions of the nearest neighbour and the next nearest neighbour distances. We compared these predictions with accurate DFT LDA calculations for supercells of moderate size. It turned out that the agreement is reasonable, which shows that the simple nearest neighbour interaction approximation made in the Keating VFF sufficiently well captures the most important aspects of the more accurate DFT picture. Then we also used the VFF model to examine the elastic constants, concluding that the composition dependence of c_{ij} exhibits a deviation from Vegard-like model in the form of sublinear bowing. This is in accordance with

suggestions already made in the literature [46, 49]. We also presented accurate quadratic function fits, which very well approximate the dependence of c_{ij} on composition, including aforementioned bowing effect. This could be used to improve the continuous models of nanostructures. Finally, we examined the influence of the mixing rules on the VFF results. It turned out that the structural properties remain virtually unaffected when one uses geometric mixing instead of arithmetic mixing. The effect on the elastic constants is larger, however it is still much lower than the typical experimental error.

Acknowledgment

This research was supported by the European Union within the European Regional Development Fund, through the grant Innovative Economy (POIG.01.01.02-00-008/08).

References

[1] Gorczyca I, Suski T, Christensen N E and Svane A 2009 *Phys. Status Solidi* c **6** S368–71
[2] Gorczyca I, Łepkowski S P, Suski T, Christensen N E and Svane A 2009 *Phys. Rev.* B **80** 075202
[3] Miyano K E, Woicik J C, Robins L H, Bouldin C E and Wickenden D K 1997 *Appl. Phys. Lett.* **70** 2108
[4] Yu K M, Shan W, Glover C J, Ridgway M C, Wong W S and Yang W 1999 *Appl. Phys. Lett.* **75** 4097
[5] Katsikini M, Pinakidou F, Paloura E C, Komninou P, Iliopoulos E, Adikimenakis A, Georgakilas A and Welter E 2008 *Phys. Status Solidi* a **205** 2593
[6] Jeffs N J, Blant A V, Cheng T S, Foxon C T, Bailey C, Harrison P G, Mosselmans J F W and Dent A J 1998 *Proc. MRS March Meeting (San Francisco)* (Pittsburg, PA: Materials Research Society)
[7] Katsikini M, Paloura E C, Boscherini F, D'Acapito F, Lioutas C B and Doppalapudi D 2003 *Nucl. Instrum. Methods Phys. Res.* B **200** 114
[8] Kachkanov V, O'Donnell K P, Martin R W, Mosselmans J F W and Pereira S 2006 *Appl. Phys. Lett.* **89** 101908
[9] Miyanaga T, Azuhata T, Matsuda S, Ishikawa Y, Sasaki S, Uruga T, Tanida H, Chichibu S F and Sota T 2007 *Phys. Rev.* B **76** 035314
[10] Łepkowski S P and Majewski J A 2004 *Solid State Commun.* **131** 763
[11] Łepkowski S P, Majewski J A and Jurczak G 2005 *Phys. Rev.* B **72** 245201
[12] Łopuszyński M and Majewski J A 2007 *Phys. Rev.* B **76** 045202
[13] Łepkowski S P 2007 *Phys. Rev.* B **75** 195303
[14] Keating P N 1966 *Phys. Rev.* **145** 637
[15] Zi J, Wan X, Wei G, Zhang K and Xie X 1996 *J. Phys.: Condens. Matter* **8** 6323
[16] Zi J, Wei G, Zhang K and Xie X 1996 *J. Phys.: Condens. Matter* **8** 6329
[17] Wei G, Zi J, Zhang K and Xie X 1997 *J. Appl. Phys.* **82** 622
[18] Bellaiche L, Wei S H and Zunger A 1997 *Phys. Rev.* B **56** 13872
[19] Mattila T and Zunger A 1999 *J. Appl. Phys.* **85** 160
[20] Saito T and Arakawa Y 1999 *Phys. Rev.* B **60** 1701
[21] Grosse F and Neugebauer J 2001 *Phys. Rev.* B **63** 085207
[22] Chen S, Gong X G and Wei S H 2008 *Phys. Rev.* B **77** 073305
[23] Xiang H J, Wei S H, Silva J L F D and Li J 2008 *Phys. Rev.* B **78** 193301
[24] Ho I and Stringfellow G B 1996 *Appl. Phys. Lett.* **69** 2701
[25] Takayama T, Yuri M, Itoh K, Baba T and Harris J 2000 *Japan. J. Appl. Phys.* **39** 5057
[26] Takayama T, Yuri M, Itoh K and Harris J J S 2001 *J. Appl. Phys.* **90** 2358
[27] Adhikari J and Kofke D A 2004 *J. Appl. Phys.* **95** 4500
[28] Karpov S Y, Podolskaya N I, Zhmakin I A and Zhmakin A I 2004 *Phys. Rev.* B **70** 235203
[29] Biswas K, Franceschetti A and Lany S 2008 *Phys. Rev.* B **78** 085212
[30] Adhikari J and Kofke D A 2004 *J. Appl. Phys.* **95** 6129
[31] Kim K, Lambrecht W R L and Segall B 1996 *Phys. Rev.* B **53** 16310
[32] Kresse G and Hafner J 1994 *Phys. Rev.* B **49** 14251
[33] Kresse G and Furthmüller J 1996 *Phys. Rev.* B **54** 11169
[34] Kresse G and Furthmüller J 1996 *Comput. Mater. Sci.* **6** 15
[35] Kresse G and Joubert D 1999 *Phys. Rev.* B **59** 1758
[36] Monkhorst H J and Pack J D 1976 *Phys. Rev.* B **13** 5188
[37] Schabel M C and Martins J L 1991 *Phys. Rev.* B **43** 11873
[38] Cai Y and Thorpe M F 1992 *Phys. Rev.* B **46** 15872
[39] Cai Y and Thorpe M F 1992 *Phys. Rev.* B **46** 15879
[40] Marques M, Teles L K, Ferreira L G, Scolfaro L M R, Furthmüller J and Bechstedt F 2006 *Phys. Rev.* B **73** 235205
[41] Ceperley D M and Alder B J 1980 *Phys. Rev. Lett.* **45** 566
[42] Vegard L 1921 *Z. Phys.* A **5** 17
[43] Kuykendall T, Ulrich P, Aloni S and Yang P 2007 *Nat. Mater.* **6** 951
[44] Thorpe M F, Jin W and Mahanti S D 1991 *Disorder in Condensed Matter Physics* ed J A Blackman and J Taguena (New York: Oxford University Press) p 22
[45] Martins J L and Zunger A 1984 *Phys. Rev.* B **30** 6217
[46] Chen A B and Sher A 1995 *Semiconductor Alloys: Physics and Materials Engineering (Microdevices)* 1st edn (New York: Plenum)
[47] Ambacher O, Majewski J, Miskys C, Link A, Hermann M, Eickhoff M, Stutzmann M, Bernardini F, Fiorentini V, Tilak V, Schaff B and Eastman L F 2002 *J. Phys.: Condens. Matter* **14** 3399
[48] As D J, Schnietz M, Schörmann J, Potthast S, Gerlach J W, Vogt J and Lischka K 2007 *Phys. Status Solidi* c **4** 2318
[49] Łopuszyński M, Bartoszek J and Majewski J A 2007 *Acta Phys. Pol.* A **112** 449
[50] Martin R M 1972 *Phys. Rev.* B **6** 4546